RP Current Trends in Engineering and Technology
Vol. 2, No. 1 (January – March 2023) pp. 1–7
e-ISSN: 2583-5491

RESEARCH PLATEAU PUBLISHERS

Cite this article: Surila, Synthesis and characterization of nanosize particles of hematite by sol-gel technique, *RP Cur. Tr. Eng. Tech*. **2** (2023) 1–7.

Original Research Article

Synthesis and characterization of nanosize particles of hematite by sol-gel technique

Surila
Department of Chemistry, Government P.G. Nehru College, Jhajjar – 124103, Haryana, India
*Corresponding author, E-mail: surilachanderbhan@gmail.com

ARTICLE HISTORY
Received: 2 Oct. 2022
Revised: 24 Dec. 2022
Accepted: 4 Jan. 2023
Published online: 8 Jan. 2023

KEYWORDS
Nanoparticles; iron oxide; sol-gel; Mossbauer; magnetization.

ABSTRACT
By using a modified sol-gel technique, hematite nanoparticles of various sizes, spanning from 22 to 56 nm, were chemically created. By using x-ray and Mössbauer measurements, it was possible to obtain and distinguish between pure alpha phase particles and particles that had an admixture of alpha and gamma phase. There are several size and phase regulating parameters. With higher annealing temperatures for the gel and higher concentrations of the compounds, the average particle size falls (citric acid). The relative proportions of the two phases are impacted by the annealing temperature, which has an impact on the magnetization of the particles. When the annealing temperature rises, the particle magnetism (M_s) and coercivity (H_c) both increase steadily. The coercivity (H_c) and the moment of the particles rise with the decrease in the size of the particles for the same relative amount of the two phases, suggesting the importance of surface effects in the magnetic behaviour.

1. Introduction

Iron (III) oxide is a practical substance for the broad study of polymorphism and the magnetic and structural phase transitions of nanoparticles from the perspective of basic research. Alpha, beta, gamma, and epsilon are the four polymorphs of amorphous Fe_2O_3 that are known to exist [1]. Hematite and maghemite minerals, which feature the hexagonal corundum structure "alpha" and cubic spinel structure "gamma," respectively, are the most prevalent polymorphs. The orthorhombic structure "epsilon" and cubic bixbyite structure "beta," as well as nanoparticles of all types, have all been produced and thoroughly studied recently [1, 2].

Epsilon and gamma type Fe_2O_3 are paramagnetic materials, while beta type Fe_2O_3 is a canted antiferromagnetic substance. At ambient temperature, the magnetic moment of bulk gamma-type Fe_2O_3 is about 430 emu/cc, whereas the magnetic moment of alpha-type Fe_2O_3 is incredibly low (about 1 emu/cc) in comparison to the gamma phase [3]. In addition to its antiferromagnetism below 960 K, α-Fe_2O_3 (hematite) also exhibits modest ferromagnetism beyond roughly 260 K ^{TM} [4]. The Morin transition is the name of this transition at lower temperatures. The antiferromagnetically aligned spins above TM are canted at an angle of 5°, which is what causes the mild ferromagnetism that is observed [5, 6]. The Morin temperature has been observed to be substantially dependent on particle size, often decreasing with it and tending to disappear below a diameter of 8 nm for spherical particles [7]. Nanoparticles of the alpha phase likewise display this behaviour.

Recent years have seen the publication of novel techniques for the production of α-Fe_2O_3 nanoparticles as well as fresh methods for their characterisation due to the appealing scientific and industrial applications of these materials. According to reports [8, 9], various preparation methods result in various phases or mixes of phases as well as various levels of size control. Furthermore, there is still disagreement regarding the relationship between the preparation route and magnetic properties like moment and coercivity. In this study, we describe a modified sol-gel approach for producing Fe_2O_3 nanoparticles (α and α+γ) and correlate the characteristics of the produced nanoparticles as functions of several preparation parameters.

2. Materials and methods

Our goal was to use the solgel method to create hematite (α-Fe_2O_3) nanoparticles and to determine the factors that affect their size. Many approaches can be used to do this, according to earlier studies. According to reports, gelation and polymerization methods were used to create nanocomposites of polypyrrole and iron oxide. In one instance [10], different concentrations of pyrrole monomer were introduced to a mixture of 2-methoxy ethanol as solvent and iron nitrate as precursor. Hematite particles were created by Matijevic and Scheiner [11] by dissolving ferric salts in hydrochloric acid and heating at 100°C. For more simplicity, we slightly adjusted the way we made these particles. As the ligand molecules, 800 ml of mono hydrated citric acid (Aldrich 98%) solution (0.05 to 0.2M) was used as the solvent, and 200 ml (0.1M) of iron nitrate $Fe(NO_3)_3.9H_2O$ (Aldrich 98%) was utilised as the precursor solution. The citric acid solution was vigorously stirred while drops of the iron solution were added. The mixture was then heated to 70°C while being vigorously stirred until the gel had formed and the water in it had evaporated. The dried gel was annealed at 180–400°C, generally producing 1.6 g of Fe_2O_3 with a size range of 22–56 nm.

We measured the average size of the particles and the crystal structure using an x-ray diffractometer (JDX-11 Jeol). The relative proportions of the alpha and gamma phases as well as the magnetic identification of the particles were studied using a commercial vibrating sample magnetometer (VSM) and Mössbauer spectroscopy.

3. Results and discussion

Analysis and characterization of sol-gel prepared particles

This article will cover two typical x-ray diffraction patterns that are illustrative of the general behaviour. Figure 1 displays exemplary data for the samples that were annealed between 180 and 250°C. This particular sample (sample #2) was created using the previously mentioned technique, with the iron nitrate and citric acid molarities both being 0.1 and the gel produced being annealed at 210°C. At 2θ = 33.2°, the major XRD peak was found, and at 2θ = 35.7°, the second significant peak. The other observed peaks were at 2θ = 41°, 49.55°, 54.25°, and 62.55°. For diverse samples corresponding to this range of annealing temperature, the relative strength of these two primary peaks ranged between 70 and 80%. The relative strengths of the two large peaks and the three minor peaks clearly suggest that alpha Fe_2O_3 is the major phase in this material, even if the 35.7° peak might be caused by either the alpha or gamma phases. For this collection of alpha Fe_2O_3 nanoparticles, the lattice constants are $a = b = 5.0356$ Å and $c = 13.7489$ Å. All of the remaining samples produced a similar pattern when annealed at temperatures below 250°C, demonstrating that they are all mostly composed of the α-Fe_2O_3 phase.

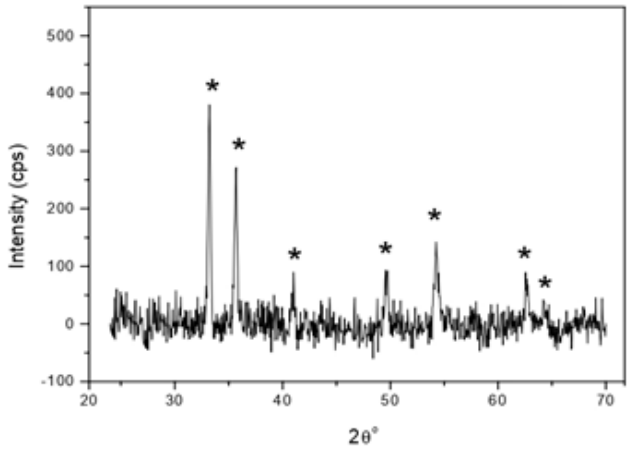

Figure 1: XRD pattern of sample #2, which was annealed at 210°C and had particles with an average size of 33 nm. (The hematite peaks are symbolised by the symbol *).

However, as shown in Figure 2, the samples that were annealed at a higher temperature (400°C) produced somewhat different patterns with the hint of some additional peaks and a clear alteration in the ratios of the two main peaks at 33.2 and 35.7°. While the positions of the two main summits remain same from Figure 1, the names of the highest and second-highest peaks have been switched. With an intensity ratio of 0.8, the 33.2° peak is now second highest and the 35.7° peak is now the most intense. The relative ratios of the two main peaks, $I_{33.2}/I_{35.7}$, are substantially less in the pure gamma phase. While both the gamma and alphas phases are present in these samples that were created at a higher temperature, we think that this is a sign that the gamma phase is probably not very abundant, which is why the smaller peaks are not evident. At 33.2 degrees, the contributions from the hematite are therefore readily apparent, but at 35.7 degrees, they overlap with the contributions from the maghemite, resulting in the peak intensity that is recorded. Thus, there is evidence that structural changes are taking place at higher annealing temperatures (250–400°C) that enable the creation of the gamma phase in addition to the alpha phase. The Mössbauer results that are addressed later provide resounding confirmation of this pattern.

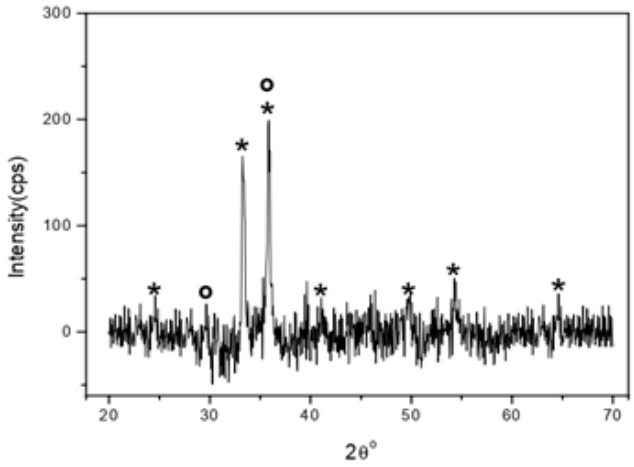

Figure 2: XRD pattern of sample #8, which was annealed at 400 oC and had particles with an average size of 33 nm. (The symbols * and o, respectively, stand for the peaks of hematite and maghemite.).

Scherrer's formula for the peak width widening as a function of the particle size was used to calculate the average particle diameter D for several specimens from the principal peaks.

$$D = \frac{k\lambda}{\beta\cos(\theta)}$$

Here λ is the x-ray wavelength (Cu Kα = 1.5418Å), k is the machine constant (0.916), β is the full width at half maximum of the peak and θ is the peak position [12].

With the aforementioned technique, we measured the average size of sample #2's particles to be 33 nm. For a resolution of $d\theta = 0.01°$ between the data points, the error in the estimated average particle size was around 2 nm. The following section discusses the specific size fluctuation with various parameters.

Size controlling parameters and their effects

We found that three parameters affected the size of the particles in the current sol-gel process. The solutions were diluted, the citric acid solution was concentrated, and the dried gel was annealed at a specific temperature. We briefly address these implications in the sections that follow.

A: We define mixtures as being more diluted if the citric acid solution to iron nitrite ratio is larger. Normally, we blended the citric acid solution and iron solution in a 1:4 ratio. The likelihood of colloidal particles in a solution interacting with one another decreases with increasing solution dilution. Hence, it would seem that combinations with higher dilution

would produce particles of smaller sizes. The size of the particles decreases from 33 nm to 27 nm when comparing the diameters of the particles produced from mixtures with the dilution ratios of 1:4 and 1:8, respectively, while maintaining all other reaction-related parameters constant. Even though there are only these two sets of distinct dilutions, the tendency here seems to be in line with what may be expected, namely that smaller sizes correspond to higher dilution.

B: The second element influencing the size of the particles is the concentration of the ligand (citric acid). Citrate ions will become more abundant as citric acid concentration rises, protecting the developing particles' surfaces against agglomeration. Hence, a rise in concentration may tend to encourage the development of particles of smaller sizes. As the concentration of citric acid increases from 0.05 to 0.2M, the particle size decreases from 56 ± 6 to 22 ± 4 nm, demonstrating this pattern (molarity).

C: The "annealing temperature" is the term used in the literature [13] to describe the temperature at which the gel was dried. The precursor, the dried gel, is purified at this temperature by the breakdown of organic molecules and other contaminants. We see that this temperature has a big impact on the size of the final product; for example, the size of the produced particles reduces from 36 to 22 nm as the annealing temperature is raised from 180 to 250^{o}C. Table 2 illustrates this. The lesser likelihood of agglomeration for the particles emerging from the colloidal gel network at higher average energies associated with the higher temperatures, according to our hypothesis, may be the cause of this reduction in size. According to the concentration of the reactants and the specific preparation method employed, a change in the annealing temperature might result in an increase or decrease in the size of the particles [13].

Magnetic measurement on the different size particles

We compressed the particles into pellets and then chopped those pellets into the appropriate sizes in order to assess their magnetic characteristics. Our measurements were primarily concerned with figuring out the magnetization of the particles as a function of their size and certain preparation conditions. The hysteresis, coercivity, and magnetization were measured. Using a commercial vibrating sample magnetometer, the DC measurements were made (VSM). Temperatures of 300 and 77K were used to study the hysteresis loops. Typical field cycling range was between ± 10kOe.

Table 1: Effect of citric acid concentration on the nanoparticles properties.

Sample No #	Concentration (M)	Size (nm)	M_s (emu/g)	H_c (Oe)
6	0.2	22	24.7	157
7	0.1	27	23.5	118
8	0.1*	33	20.3	59
9	0.05	56	25.3	23

H_c is the coercivity, while M_s is the saturation magnetization. All of these samples were prepared at a dilution ratio of 1:4 with the exception of the sample that is highlighted starred*, which had a ratio of 1:8. Note that all of these samples were annealed at 400^{o}C.

Table 2: Effect of annealing temperature on the nanoparticles properties.

Sample No #	Temperature (^{o}C)	Size (nm)	M_s (emu/g)	H_c (Oe)
1	180	36	0.3	---
2	210	33	3.7	39
3	230	31	5.1	43
4	250	24	12	81
5	400	22	25	160

H_c is the coercivity, while M_s is the saturation magnetization. All samples were prepared at a citric acid concentration of 0.1 M.

The magnetization loop of sample #2 (33 nm), which was created (annealed) at 210^{o}C and as previously said, the x-ray results demonstrate the presence of the phase, is shown in Figure 3. Above 260 K, it should exhibit the modest ferromagnetism associated with this phase. At room temperature, the magnetization loop exhibits considerable hysteresis (H_c = 39Oe) and a magnetic moment of 3.66 emu/g (6.45 emu/cc). At 77 K, the coercivity went from 39 to 357Oe, whereas the moment is somewhat bigger (3.72 emu/g; 6.55 emu/cc). It is clear that the hysteresis loop has a constricted shape at ambient temperature and a symmetric shape at 77 K. Usually, materials having a mix of a soft and hard magnetic phase are found to have constrained loops [3]. The observed reaction may therefore, at room temperature, result from the interaction of the alpha and gamma phases, the alpha phase having a lot stronger coercivity but a much lower moment and the gamma phase being a soft phase with a much larger moment. On the other hand, the alpha phase is completely antiferromagnetic and virtually has the gamma phase's magnetism at low temperatures. The rise in the gamma phase's anisotropy energy may be the cause of the coercivity increase at lower temperatures.

The magnetization values for samples #1 and #12 should be contrasted with those in the table above. Sample #1 was created using citric acid and iron nitrate in 0.1M concentrations, and it was then annealed at 180oC. Sample #12 was made by ageing the dry precursors (gel) at 90°C for roughly 16 hours in an open environment with 0.2M citric acid and 0.1M iron nitrate concentration. Keep in mind that no annealing at higher temperatures was done. The lowest moments were found in these two samples, which were 0.3 emu/g (#1) and 0.89 emu/g (#12), respectively. These values are in excellent agreement with previous studies [4, 14] for pure hematite nanoparticles. On these samples, Mössbauer analysis revealed peaks only matching to the alpha phase. However, for the additional samples created by varying one of the parameters, i.e. We found magnetizations between 3 and 25 emu/g, indicating a greater fraction of the ferromagnetic phase, either by concentration or temperature. At room temperature, these particles have a coercivity that ranges from 23 to 157Oe. In contrast to samples with smaller moments, those with higher moments show a stronger tendency towards saturation (a lower high field slope of the M(H) curve). They are shown in Figures 3 and 4. This is in line with the gamma phase's lesser anisotropy compared to the alpha phase, which is particularly challenging to saturate. The non-constricted loops were seen in the particles with bigger moments, most likely because of the gamma phase's predominance. As a result, constricted loops

only manifest when a negligible amount of gamma phase (5–6%) coexists with the alpha phase. This is a discussion of how preparation parameters and size affect variations in particle moments.

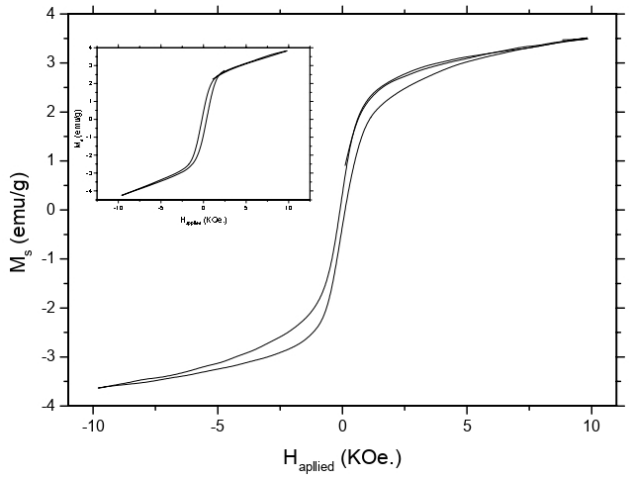

Figure 3: M-H loop of sample #2 (33 nm) at 300 K (H_c = 39Oe). (Inset) M-H loop of sample #2 (33 nm) at 77 K (Hc = 357Oe).

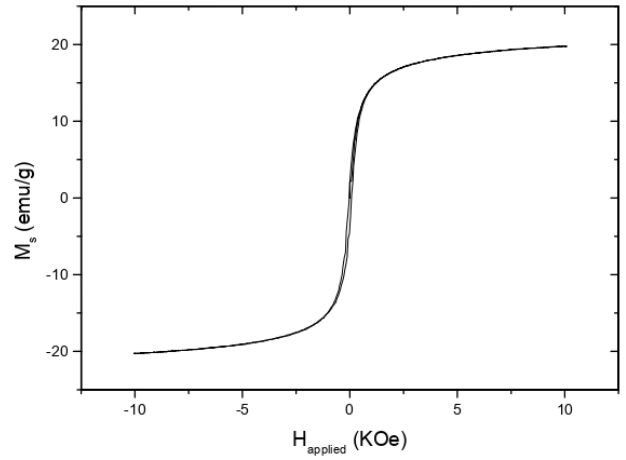

Figure 4: M-H loop of sample No. # 8 annealed at 400°C.

Discussion of magnetization

The magnetizations of our samples, which should be 1 emu/cc for pure hematite but are typically in the range of 6 to 90 emu/cc depending on various preparation factors, were generally significantly higher than predicted. This is explained by the fact that our particles contain trace amounts of the ferromagnetic gamma phase. It should be noted that a very tiny amount of γ-Fe_2O_3 is sufficient to generate a very considerable rise as compared to the moment of pure hematite due to the very large moment of γ-Fe_2O_3 (approximately 500 times) [3] as compared to α-Fe_2O_3. For instance, using the typical values of the moments of the two phases in the bulk, 0.2 emu/g for the alpha phase and 85 emu/g for the γ-Fe_2O_3 phase, we computed the proportion of γ-Fe_2O_3 in the sample (#2) whose average magnetization was (3.66 emu/g). Hence the average moment for a sample with x and 1–x fractions of α-Fe_2O_3 and γ-Fe_2O_3 respectively would be $M_s = (x)(M_{Fe_2O_3}) + (1-x)(M_{\gamma-Fe_2O_3})$.

We discover that the leftover alpha phase particles and around 4% of the γ-Fe_2O_3 phase (1–x = 0.04) would be sufficient to produce the observed signal. Inferring from the bulk values of the moments of the two phases, we therefore calculate that Sample #2, with M_s =3.66 emu/g, comprised 96% hematite and 4% γ-Fe_2O_3, respectively.

It is clear that the moment is higher for samples that were annealed at 400°C, ranging from 70 to 90 emu/cc (20–25 emu/g) depending on the molarity of the citric acid. One such instance (sample #8, M_s = 20.3 emu/g) had a proportion of γ-Fe_2O_3 that was calculated to be around 24%. Figure 2 depicts the XRD pattern for these particles and highlights the peaks associated with the γ-Fe_2O_3 phase.

The existence of the gamma phase was confirmed by Mössbauer measurements on the same sample (#8). According to the research, compositions with higher annealing temperatures enable x-ray diffraction to measure the amount of γ-Fe_2O_3. Consequently, we draw the conclusion that the fraction of γ-Fe_2O_3 is larger in the samples that were annealed at the higher temperatures in this range.

Effect of size on M_s and H_c

This conversation can be divided into two sections.

1: Particles whose size variation was produced by a change in citric acid concentration (ligand molecules).

2: Particles with size variation brought on by annealing temperature changes.

A: At 400°C, all of these particles underwent annealing. Although there does seem to be a minor drop in the moment with increasing size in the region 22-33 nm, we do not see significant changes in the magnetization with nanoparticle size in the range 22 to 56 nm.

Table 1 displays this information, and we can see that the moment is between 20.3 emu/g and 25.3 emu/g. Hence, adjustments in the citric acid (ligand) concentration (for 400°C anneal) do not seem to appreciably alter the relative amounts of the two phases, but they do have a major impact on the particle sizes.

The coercivity's relationship to size is depicted in Figure 5 and is seen to be quite consistent, rising steadily as particle size decreases. The size decreases from 56 to 22 nm, causing a shift that is fairly significant and ranges from 23 to 157Oe.

B: Now, while maintaining a constant ligand concentration, we analyse the magnetic behaviour of particles whose size variation has been achieved by varying the annealing temperature. Figure 6 depicts the variation in coercivity and magnetic moment with annealing temperature, and Table 2 provides more information on the influence on the sizes thus achieved.

As the size of the particles grows, we see that the moment obviously decreases. This shows that the percentage of the ferromagnetic phase is decreasing as particle size increases. The published behaviour [15] states that the gamma phase is stable for particles with diameters d < 30 nm and the alpha phase for particles with larger sizes. This tendency is consistent with that behaviour. The sample in this series with the highest moment clearly showed the presence of the gamma phase. Consequently, while the alpha phase is dominating, our data demonstrate that its amount continually declines as the size drops from 33 to 22 nm.

According to Table 2's data, lowering particle size through heat treatment at higher temperatures causes an increase in magnetization as well as a coercivity increase from 39 to 162Oe.

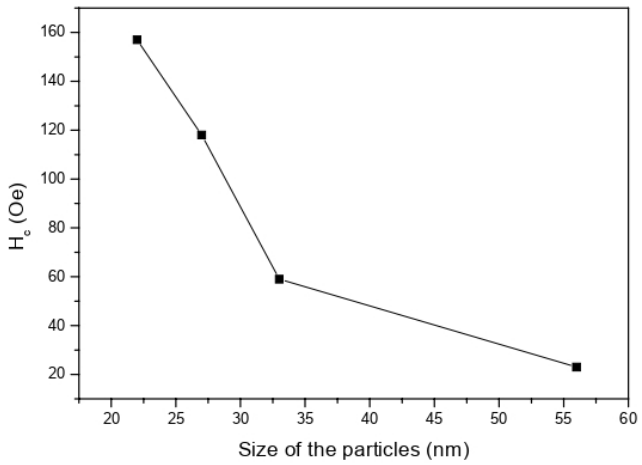

Figure 5: Influence of particle size on coercivity when reactant concentration is changed to produce different particle sizes (In Table 1).

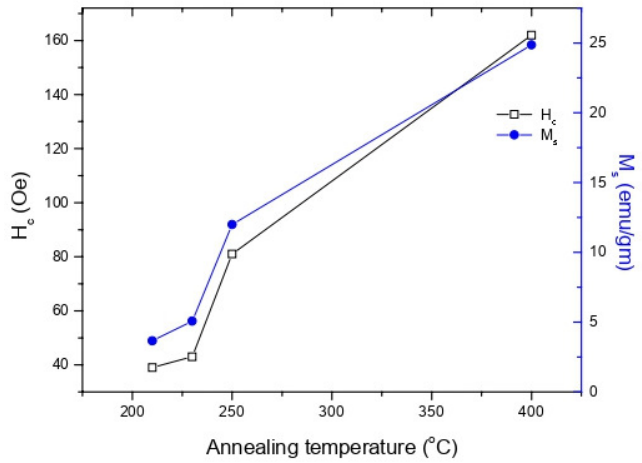

Figure 6: Size variation was obtained by varying the annealing temperature. M_s (emu/gm) and H_c (Oe) vs. temperature. (Details are in Table 2).

Hence, both techniques for creating size variations share the tendency for coercivity to rise as nanoparticle size decreases. Many studies [16–18] have reported that the coercivity tends to decline when single domain nanoparticle size increases (over a critical size). Chen et al [17] explain this behaviour in nanoparticles in terms of an energy barrier (ΔE) for the rotation of the moments that depends on the surface area of the particle, $\Delta E = K_s S$. Here K_s is the surface anisotropy constant and S the surface area of the particle. This has been shown to lead to a coercivity that decreases with the size of the particles as $H_c \sim 1/d$. Consequently, it is clear that the observed increase in the coercivity of the particles as their size decreases is a reflection of the surface's growing significance in defining anisotropy and, by extension, coercivity.

Mössbauer studies

As mentioned above, magnetometry was used to identify the phases and their relative proportions as they were formed under various preparation conditions. Mössbauer measurements were used on a number of representative samples to further verify this. A ^{57}Co (Rh-matrix) source with transmission geometry and an initial activity of 25 mCi was used to gather the Mössbauer data. Using the computer code Mos90, the data were fitted. All spectra were collected at room temperature, and fitting was done under the assumption that every peak had a Lorentzian shape.

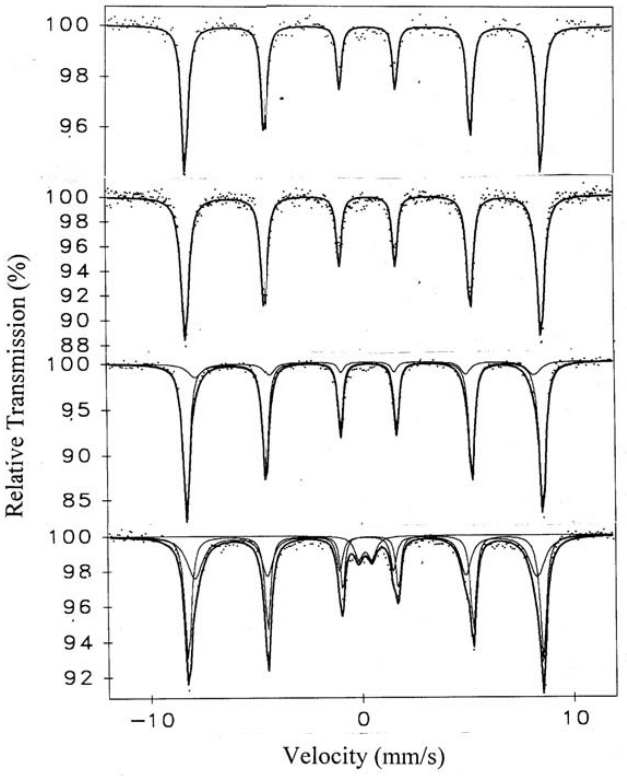

Figure 7: Samples #12, #1, #2, and #8's Mössbauer spectra, as stated in the text (top to bottom). The data's best fit is given.

Figure 7 displays the Mössbauer spectra for samples #1 and #12. The characteristics of the best-fit spectra clearly show that just α-Fe_2O_3 is present. These samples include no indication of γ-Fe_2O_3 or any other iron phase. This agrees with the earlier discussed magnetization measurements. However, the α-Fe_2O_3 and γ-Fe_2O_3 phases of samples #2 and #8 could be distinguished from the Mössbauer spectrum. Table 3 reports the characteristics of the best-fitted spectrum and the proportion of the two indicated phases for each sample. The fractional area under the various peaks is used to estimate the percentage of the phases. Two sub-spectra, representing α Fe_2O_3 (84% of the total sample) and γ-Fe_2O_3 (16%), were present in the spectrum for sample #2. The major spectrum of sample #8 had three sub-spectra, including α-Fe_2O_3 (51% of the whole sample), γ-Fe_2O_3 (43%), and a doublet that has been identified as γ-Fe_2O_3 (6%), all of which were present in the main spectrum.

Hence, with reference to the relative fractions of the alpha and gamma phases obtained under various preparation conditions, the results of magnetometry and Mössbauer are qualitatively similar. As a result, we observe that with our processing method, pure alpha phase can be achieved, as demonstrated by the Mössbauer. Given that we employed bulk magnetization values to estimate the fraction of the two phases using magnetometery, it is not surprising that the quantity of

gamma phase estimated by magnetization and Mössbauer techniques for samples #2 and #8 respectively differed.

Table 3: Mössbauer spectroscopy of various samples of sol-gel-prepared nanoparticles.

Sample No. #	H_{eff} KOe	QS (Δ) mm/s	IS (δ) mm/s	LW (Γ) mm/s	Area (%)	Phase
12	522	– 0.213	0.37	0.35	100	α - Fe_2O_3
1	522	– 0.206	0.37	0.42	100	α - Fe_2O_3
2	523	– 0.209	0.37	0.35	84	α - Fe_2O_3
	498	– 0.206	0.37	0.76	16	γ -Fe_2O_3
8	521	– 0.238	0.386	0.346	51	α - Fe_2O_3
	502	–0.03	0.308	0.88	43	γ -Fe_2O_3
	**	–0.63	0.27	0.50	6	γ -Fe_2O_3

Mössbauer parameters: Effective magnetic field (H_{eff}), quadrupole splitting (Δ), isomer shift (δ), line width (Γ) and area under the peak.

4. Conclusions

We note that under the following two circumstances, a modified sol-gel approach yields the best results for producing alpha phase particles: (i) Particles that were created by ageing the dry precursors (gel) at 90°C for approximately 16 hours in an open environment while using 0.2 M citric acid and 0.1 M iron nitrate. Notably, no further temperature annealing at higher temperatures was necessary, in contrast to some other approaches. (12^{th} example). (ii) Pure alpha phase particles were produced for samples that were annealed at high temperatures at a temperature of 180°C and 0.1 M concentrations of both citric acid and iron nitrate.

We notice that size fluctuation can occur without significantly changing the amount of the gamma phase when reactant concentrations are changed. On the other hand, changes in anneal temperature between 180 and 400°C cause similar changes in size but are accompanied by significant changes in the proportion of the gamma phase that is present.

Regardless of the method used to change the particle sizes or the quantity of gamma phase present, we find that the coercivity decreases as particle size increases. We relate the decreasing trend of coercivity with size to the greater significance of surface anisotropy for smaller size particles. In systems including nanoparticles, high surface anisotropy values are very typical. We also discover that the creation of narrower hysteresis loops results from the presence of minute gamma phase traces that are invisible by x-ray measurements in the magnetization measurements. It is important to note that the loop constriction disappears at low temperatures, most likely because the weak ferromagnetism in the alpha phase is absent.

We get to the conclusion that as the annealing temperature is raised, the particle size decreases. However, by altering this value, we can only successfully lower the particle size up to a range of temperatures, namely up to 250°C, where the size produced is 24 nm. Above this point, the fraction of γ-Fe_2O_3 begins to rise without a significant change in particle size, as opposed to the anticipated drop in size.

We observe that the association between sizes and the gamma phase is highly evident in samples where size control was achieved by adjusting the temperature. At higher temperatures, smaller particles are produced that are more ferromagnetic and have a greater proportion of the gamma phase. Ayyub et al. [15] have examined how size and ferromagnetic behaviour are related. They claim that the ferromagnetic phase is stable for particle sizes lower than $d \sim 30$ nm. In our situation, the higher anneal temperature ($210 < T < 400$°C) not only results in lower particle sizes but also aids in gamma phase stabilisation. With one caveat, our findings agree with the discussion above. This criterion is not met by the smaller-sized particles produced by concentration fluctuations because, for particles formed at 400°C, the moment is mostly independent of size. The concentration of the critical acid solution, which is both the ligand and the substance that regulates the solution's pH, increases together with a decreasing trend in the size of the particles.

In conclusion, we successfully created alpha Fe_2O_3 nanoparticles using the sol-gel method, and we investigated their magnetic properties. The correlation between the particle size dependence on various preparation parameters and the study and logical justification of the size dependence of the coercivity and moment. To determine how to modify the size beyond these boundaries and to be able to separate the two phases in the oxide nanoparticles, more research is necessary.

Acknowledgements

The authors would like to thank Prof. Ashish Agarwal, Department of Physics, Guru Jambheshwar University of Science & Technology, Hisar – 125001 (Haryana) India for providing the necessary facilities to synthesize the materials and their characterization in their Materials Science Laboratory.

References

[1] R. Zboril, M. Mashlan, D. Petridis, Iron (III) Oxides from Thermal Processes Synthesis, Structural and Magnetic Properties, Mossbauer Spectroscopy Characterization, and Applications, *Chemistry of Materials* **14** (2002) 969-982.

[2] R. Zboril, M. Mashlan, D. Krausova, P. Pikal, Cubic β-Fe_2O_3 as the product of the thermal decomposition of $Fe_2(SO_4)_3$, *Hyperfine Interact* **120** (1999) 497-501.

[3] R. Skomski, J.M.D. Coey, *Permanent Magnetism*, Institute of Physics Publishing Ltd. (1999).

[4] R.D. Zysler, M. Vasquez-Mansilla, C. Arciprete, M. Dimitrijewits, D. Rodriguez-Sierra, C. Saragovi, Structure and magnetic properties of thermally treated nanohematite, *J. Magn. Magn. Mater*. **224** (2001) 39-48.

[5] C.G. Shull, W.A. Strauser, E.O. Wollan, Neutron diffraction by paramagnetic and antiferromagnetic substances, *Phys. Rev. B* **83** (1951) 333-345.

[6] C. Guilland, Magnetic properties of α -Fe_2O_3, *J. Phys. Radium* **12** (1951) 489.

[7] N. Amin, S. Arajs, Morin temperature of annealed submicronic α-Fe_2O_3 particles, *Phys. Rev. B* **35** (1987) 4810.

[8] C. Chaneac, Structural and magnetic characterization of α-Fe_2O_3, *J. Solid State Chem.* **139** (1998) 93-104.

[9] P. Chauhan, S. Annapoorni, S.K. Trikha, Humidity-sensing properties of nanocrystalline haematite thin films prepared by sol-gel processing, *Thin Solid Films* **346** (1999) 266-268.

[10] K. Suri, S. Annapoorni, R.P. Tandon, Phase change induced

by polypyrrole in iron-oxide polypyrrole nanocomposite, *Bull. Mater. Sci*. **24** (2001) 563-567.
[11] C.R. Martin, Nanomaterials: A membrane-based synthetic approach, *Science* **266** (1994) 1961-1966.
[12] B.D. Cullity, *Elements of X-ray Differaction*, 2nd Edition, Eddison-Wesley Publishing Inc. (1978).
[13] M.Z. Dang, D.G. Rancourt, J.E. Dutrizac, G. Lamarche, R. Provencher, Interplay of surface conditions, particle size, stoichiometry, cell parameters, and magnetism in synthetic hematite-like materials, *Hyperfne Interactions* **117** (1998) 271-319.
[14] T.P. Raming, A.J.A. Winnubst, C.M. van Kats, A.P. Philipse, The synthesis and magnetic properties of nanosized hematite (α-Fe_2O_3) Particles, *J. Colloid Interface Sci*. **249** (2002) 346-350.
[15] S. Mitra, S. Das, S. Basu, P. Sahu, K. Mandal, Shape- and field-dependent Morin transitions in structured α-Fe_2O_3, *J. Magnet. Magnetic Mater*. **321** (2009) 2925-2931.
[16] H. Dong, A. Meininger, H. Jiang, K.S. Moon, C.P. Wong, Magnetic nanocomposite for potential ultrahigh frequency microelectronic application, *J. Electron. Mater*. **36** (2007) 593–597.
[17] P.G. Bercoff, H.R. Bertorello, M.I. Oliva, Memory effect of ball-milled and annealed nanosized hematite, *Physica B: Condensed Matter* **398** (2007) 204-207.
[18] R.D. Zysler, D. Fiorani, A.M. Testa, L. Suber, E. Agostinelli, M. Godinho, Size dependence of the spin-flop transition in hematite nanoparticles, *Phys. Rev. B* **68** (2003) 212408.